Fermi surface in the hidden-order state of URu_2Si_2 under intense pulsed magnetic fields up to 81 T

G. W. Scheerer,[1] W. Knafo,[1] D. Aoki,[2,3] M. Nardone,[1] A. Zitouni,[1] J. Béard,[1] J. Billette,[1] J. Barata,[1] C. Jaudet,[1] M. Suleiman,[1] P. Frings,[1] L. Drigo,[1] A. Audouard,[1] T. D. Matsuda,[4] A. Pourret,[2] G. Knebel,[2] and J. Flouquet[2]

[1]*Laboratoire National des Champs Magnétiques Intenses, CNRS-INSA-UJF-UPS, 143 Avenue de Rangueil, F-31400 Toulouse, France*

[2]*Institut Nanosciences et Cryogénie, SPSMS, UMR-E CEA/UJF-Grenoble 1, INAC, Grenoble, F-38054, France*

[3]*Institute for Materials Research, Tohoku University, Oarai, Ibaraki, 311-1313, Japan*

[4]*Advanced Science Research Center, Japan Atomic Energy Agency, Tokai, Ibaraki 319-1195, Japan*

(Received 4 November 2013; revised manuscript received 13 February 2014; published 7 April 2014)

We present measurements of the resistivity $\rho_{x,x}$ of URu_2Si_2 high-quality single crystals in pulsed high magnetic fields up to 81 T at a temperature of 1.4 K and up to 60 T at temperatures down to 100 mK. For a field **H** applied along the magnetic easy axis **c**, a strong sample dependence of the low-temperature resistivity in the hidden-order phase is attributed to a high carrier mobility. The interplay between the magnetic and orbital properties is emphasized by the angle dependence of the phase diagram, where magnetic transition fields and crossover fields related to the Fermi surface properties follow a $1/\cos\theta$ law, θ being the angle between **H** and **c**. For **H** ∥ **c**, a crossover defined at a kink of $\rho_{x,x}$, as initially reported in [Shishido, Phys. Rev. Lett. **102**, 156403 (2009)], is found to be strongly sample dependent: its characteristic field $\mu_0 H^*$ varies from ≃20 T in our best sample with a residual resistivity ratio RRR = $\rho_{x,x}(300\,\mathrm{K})/\,\rho_{x,x}(2\,\mathrm{K})$ of 225 to ≃25 T in a sample with a RRR of 90. A second crossover is defined at the maximum of $\rho_{x,x}$ at the sample-independent low-temperature (LT) characteristic field $\mu_0 H^{\mathrm{LT}}_{\rho,\mathrm{max}} \simeq 30$ T. Fourier analyses of Shubnikov-de Haas oscillations show that $H^{\mathrm{LT}}_{\rho,\mathrm{max}}$ coincides with a sudden modification of the Fermi surface, while H^* lies in a regime where the Fermi surface is smoothly modified. For **H** ∥ **a**, (i) no phase transition is observed at low temperature and the system remains in the hidden-order phase up to 81 T, (ii) quantum oscillations surviving up to 7 K are related to a new orbit observed at the frequency $F_\lambda \simeq 1350$ T and associated with a low effective mass $m^*_\lambda = (1 \pm 0.5)m_0$, where m_0 is the free electron mass, and (iii) no Fermi surface modification occurs up to 81 T.

DOI: 10.1103/PhysRevB.89.165107 PACS number(s): 71.18.+y, 71.27.+a, 75.30.Kz, 72.15.−v

I. INTRODUCTION

After more than 20 years of investigations, the heavy-fermion URu_2Si_2 remains an unsolved issue due to its "hidden-order" phase developing below $T_0 = 17.5$ K, for which the order parameter has still not been identified [1–6]. This system is characterized by an Ising anisotropy, with the easy magnetic axis **c** in the tetragonal structure, resulting in anisotropic electronic properties (magnetic susceptibility [2,5,7], resistivity [8,9], etc.). Superconductivity, whose upper critical field is anisotropic too, sets in below $T_{\mathrm{sc}} \simeq 1.5$ K [3,4,9,10]. Hydrostatic pressure drives the system through a first-order phase transition at $p_c = 0.5$ GPa to an antiferromagnetic ground state [11–13]. A high magnetic field applied along the **c** axis also induces a cascade of first-order transitions at the fields $\mu_0 H_1 \simeq 35$ T, $\mu_0 H_2 \simeq 37$ T, and $\mu_0 H_3 \simeq 39$ T, which were probed over the last years using a wide range of experimental techniques: magnetization [14–17], ultrasonic velocity [18–20], resistivity [14,17,21], heat capacity [22], dilatometry [23], and thermoelectricity [24,25]. The hidden-order phase is destabilized at H_1 and a polarized paramagnetic state is obtained above H_3. Between H_1 and H_3, intermediate magnetic phases are delimited by the critical field H_2. As determined recently for Rh-doped URu_2Si_2 [26], antiferromagnetic long-range ordering develops in the intermediate phases of URu_2Si_2 between 35 and 39 T. At low temperature (LT), a maximum of the magnetoresistivity at $\mu_0 H^{\mathrm{LT}}_{\rho,\mathrm{max}} \simeq 30$ T is associated with a Fermi surface modification inside the hidden-order phase [17]. At high temperature, a crossover leads to maxima at $T_{\rho,\mathrm{max}} \simeq 40$ K in the electronic, i.e., nonphononic, term of the resistivity and at $T_{\chi,\mathrm{max}} \simeq 55$ K in the susceptibility, which are related to intersite electronic correlations [17]. The suppression of these high-temperature scales at 35 T is connected to the destabilization of the hidden-order phase and to the setup of a high-field polarized regime (see also Ref. [27]). When the field rotates from the **c** to the **a** axis, the complete phase diagram is pushed towards higher field scales [28–30].

URu_2Si_2 is a compensated semimetal at low temperatures [31,32], for which a sudden reconstruction of the Fermi surface [7,33–36] occurs at the onset at T_0 of the hidden-order phase. Hall effect [7,31], thermoelectric power [37], and heat capacity [37] measurements have further shown that entering in the hidden-order phase induces a strong reduction of the charge carrier number, while an enhanced Nernst effect [37] and a strong field-induced variation of the resistivity [17] indicate a highly increased carrier mobility in the hidden-order phase. For **H** ∥ **a**, a sudden suppression of the field-dependence of the resistivity for $T > T_0$ is due to a significant loss of the carrier mobility [17]. The Fermi surface of URu_2Si_2 in its hidden-order phase is partly known from quantum oscillation experiments [9,38–43], which revealed four Fermi surface sheets associated with the frequencies $F_\eta \simeq 93$ T, $F_\gamma \simeq 200$ T, $F_\beta \simeq 425$ T, and $F_\alpha \simeq 1065$ T for **H** ∥ **c**. The Sommerfeld coefficient $\gamma_{\mathrm{FS}} \simeq 37.5$ mJ/mol K^2 estimated from these Fermi surface (FS) measurements [41] corresponds to 55% of the Sommerfeld coefficient $\gamma_{Cp} \simeq 65$ mJ/mol K^2 extracted from specific heat data [4]. In the light of band structure calculations, it is not clear whether an electron or a hole Fermi surface is missing from the quantum oscillations experiments: while Oppeneer *et al.* [44] find that a large hole Fermi surface

is missing, Ikeda *et al.* [45] find out that a heavy-electron Fermi surface is missing, in accordance with charge and transport measurements. Recently, a heavy-electron Fermi surface branch has been reported from cyclotron resonance experiments [46,47] and was estimated to account for almost 30% of the Sommerfeld coefficient determined from the specific heat, suggesting that only 20% of the Fermi surface would remain unknown. In a high field applied along **c**, Fermi surface modifications have been reported in Shubnikov-de Haas (SdH) oscillations spectra [29,42,43,48,49]. We note that slight discrepancies are found between the Fermi surface frequencies extracted from the different sets of high-field quantum oscillations measurements [29,42,43,48]. In particular, the new frequency $F_\varepsilon \simeq 1300$ T associated with a light mass $m_\varepsilon = 2.7m_0$ reported in Hall resistivity above 20 T by Shishido *et al.* [48] has not been reproduced yet.

We present here a study of the resistivity of high-quality URu_2Si_2 single crystals in high magnetic fields up to 60 T at temperatures down to 100 mK and in fields up to 81 T at 1.4 K. Experimental details are given in Sec. II. In Sec. III, measurements with the magnetic field applied along the magnetic easy axis **c** are presented. The strong sample-dependence of the magnetoresistivity in the hidden-order state is characterized carefully. A widespread study of the resistivity in various configurations is presented in Sec. IV: the effect of a magnetic field rotating in the (**a**,**c**) and (**a**,**a**) planes is investigated for both transverse and longitudinal configurations (electrical contacts perpendicular or parallel, respectively, to the field direction). The angle dependence of the phase transitions H_1, H_2, H_3, and crossovers H^* and $H^{\mathrm{LT}}_{\rho,\mathrm{max}}$ is presented. In Sec. V, Shubnikov-de Haas oscillations are investigated and permit to probe the high-field Fermi surface. For $\mathbf{H} \parallel \mathbf{c}$, magnetic-field-induced Fermi surface modifications are observed inside the hidden-order phase. For $\mathbf{H} \parallel \mathbf{a}$, quantum oscillations from the branches γ and α, and from a new light-mass branch λ are observed; they indicate that the Fermi surface is not modified in magnetic fields up to 81 T. By extending our work published in Ref. [17] to lower temperatures, higher fields, and new field orientations, this study provides further evidences of the interplay between magnetism, Fermi surface reconstructions, and the hidden-order in URu_2Si_2.

II. EXPERIMENTAL DETAILS

We have measured the resistivity of two high-quality single crystals of URu_2Si_2 grown by the Czochralski technique in a tetra-arc furnace. Details about the crystal growth can be found in Ref. [50]. The high-field electrical resistivity $\rho_{x,x}$ was investigated by the four-contact method using the lock-in technique, at frequencies from 40 to 70 kHz. The electric current I and voltage U have been applied and measured, respectively, along the [100] direction. Due to the superconducting transition at $T_{\mathrm{sc}} = 1.5$ K, it is quite difficult to extract the residual resistivity $\rho^0_{x,x}$ from an extrapolation in the limit $T \to 0$ of the normal nonsuperconducting resistivity of high-quality URu_2Si_2 single crystals, as those studied here. To compare samples, it is more convenient to consider, as proposed in Ref. [51], the residual resistivity ratio $\mathrm{RRR} = \rho_{x,x}(300\,\mathrm{K})/\,\rho_{x,x}(2\,\mathrm{K})$ defined at zero field by the ratio of the resistivities at 300 K and 2 K, i.e., just above the superconducting temperature. Within this criteria, we extract RRRs which reach $\simeq$90 and $\simeq$225, respectively, for the samples 1 and 2 studied here, indicating their very high quality (see Ref. [51] for a study of the sample-dependence of URu_2Si_2 single crystals properties). Pulsed magnetic field experiments were done at the Laboratoire National des Champs Magnétiques Intenses of Toulouse (LNCMI-T), France. Pulsed fields have been generated either by 6-mm-bore 60-T or 70-T magnets with a pulse duration of 150 ms, or by 20-mm-bore 60-T magnets with a pulse duration of 300 ms. A magnetic field up to 81 T has been generated by a new double coil [52], made of an outer coil delivering a long pulse of 250 ms up to 30 T and an inner coil delivering a short pulse of 75 ms from 30 to 81 T, which allows a unique duration of the pulse of 10.2 ms above 70 T [52]. Standard ^{4}He cryostats, as well as a home-made nonmetallic ^{3}He-^{4}He-dilution fridge specially designed for the pulsed magnetic fields have been used to reach temperatures down to 1.4 K and 100 mK, in magnetic fields up to 81 and 60 T, respectively. Electrical transport probes with static or rotating sample support have been used to study the samples properties in different configurations of the field: the transverse configurations ($\mathbf{H} \parallel \mathbf{c}$; $\mathbf{I},\mathbf{U} \perp \mathbf{H}$) and ($\mathbf{H} \parallel \mathbf{a}$; $\mathbf{I},\mathbf{U} \perp \mathbf{H}$) have been probed using a static support, while configurations with **H** applied along various directions in the (**a**,**c**) and (**a**,**a**) planes have been investigated using a rotation probe. Complementarily, the resistivity of sample 2 has been studied at $T = 32$ mK in a transversal configuration for $\mu_0 H$ up to 13 T rotating in the (**a**,**c**) plane. The Shubnikov-de Haas oscillations and their frequencies extracted from this "low-field" experiment—not shown here—are in perfect agreement with those published in Ref. [41]. Quantum oscillations were all analyzed using a Hanning window function [53].

III. SAMPLE-DEPENDENCE OF THE HIGH-FIELD RESISTIVITY

Figure 1(a) presents, at $T = 100$ mK and 1.4 K, the transverse resistivity $\rho_{x,x}$ of two URu_2Si_2 samples of different qualities [samples 1 (RRR = 90) and 2 (RRR = 225) measured here and a third sample (RRR = 35) measured by Levallois *et al.* [32] versus a magnetic field applied along the **c** axis. This plot extends to sub-kelvin temperature the study performed on samples 1 and 2 above 1.4 K in Ref. [17], where the (H,T) phase diagram has been extracted from resistivity and magnetization data. Superconductivity develops below $T_{\mathrm{sc}} = 1.5$ K and leads to $\rho_{x,x} = 0$ for $\mu_0 H < \mu_0 H_{c2} \simeq 2.5$ T at $T = 100$ mK. Figures 1(b) and 1(c) focus on the resistivity of samples 1 and 2 at $T = 1.4$ K and 100 mK, respectively, in the field range $34 \leqslant \mu_0 H \leqslant 40$ T. At $T = 1.4$ K, $\rho_{x,x}$ is almost sample-independent for $\mu_0 H > \mu_0 H_1 = 35$ T and sharp steps are observed at the first-order transition fields H_1, H_2, and H_3. However, at $T = 100$ mK, $\rho_{x,x}$ becomes sample dependent also in the field range $H > H_1$. While $\rho_{x,x}$ of sample 1 is almost the same at 100 mK as at 1.4 K, $\rho_{x,x}$ of sample 2 is strongly modified at 100 mK, the transition fields H_1, H_2, and H_3 being more difficult to define, in particular for increasing field, than at 1.4 K. Knowing that sample 2 has the highest RRR, and thus the highest electronic mean free path, this result indicates an interplay between the cyclotron motion of the electrons and their scattering on the magnetic ions.

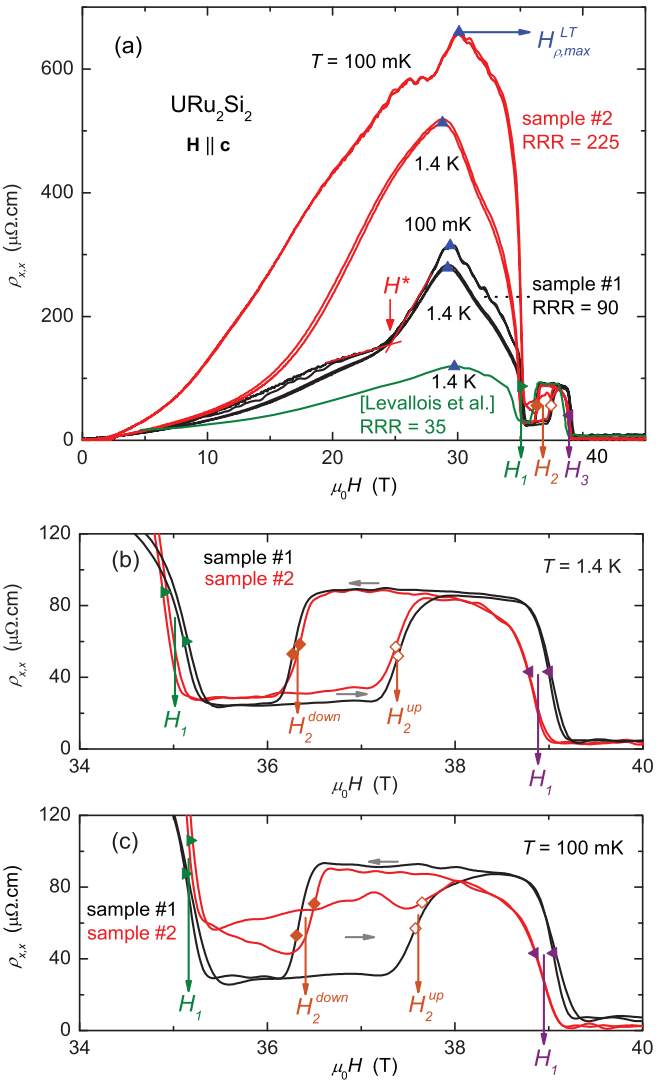

FIG. 1. (Color online) (a) Transverse resistivity $\rho_{x,x}$ vs **H** applied along **c** of samples 1 and 2 at $T = 100$ mK and 1.4 K and of a third sample measured by Levallois *et al.* [32] at $T = 1.4$ K. Zoom on $\rho_{x,x}(H)$ of samples 1 and 2 for $\mathbf{H} \parallel \mathbf{c}$ between 34 and 40 T at (b) $T = 1.4$ K and (c) 100 mK. The grey arrows indicate the rise and fall of the pulsed field.

In a compensated electron-hole two-band picture, the field-induced variation of the resistivity can be approximated at low fields by

$$\Delta\rho(H)/\rho(H=0) = \mu_e\mu_h(\mu_0 H)^2, \qquad (1)$$

where μ_e and μ_h are the electron and hole mobilities, respectively [54–56]. As shown in Figure 2(a), the resistivities $\rho_{x,x}$ of samples 1 and 2 show, in agreement with previous studies [31,32], a field-dependence close to $\propto H^2$ at $T = 100$ mK for $\mu_0 H_{c,2} \simeq 2.5\ \mathrm{T} < \mu_0 H < 10$ T. Clear deviations from an H^2 behavior are observed at higher fields, being presumably related to the complex multiband structure of the Fermi surface [44,45]. In the following, we consider the zero-field value $\rho^n_{x,x}(H=0)$ and the field-dependent term $\Delta\rho_{x,x} = \rho_{x,x} - \rho^n_{x,x}(H=0)$ of the resistivity in the normal nonsuperconducting state: below $T_{sc} = 1.5$ K, $\rho^n_{x,x}(H=0)$ of a virtual normal state was estimated by extrapolating to the low temperatures a $T^{1.5}$ law preliminarily fitted to $\rho_{x,x}(T)$ above $T_{sc} = 1.5$ K (see also Ref. [51]). From fits of $\Delta\rho_{x,x}/\rho^n_{x,x}(H=0)$ versus H^2 to Eq. (1), we extract the mobility averaged over the different bands $\mu = \langle\sqrt{\mu_e\mu_h}\rangle$, which reaches 4.5×10^3 and 1.9×10^4 cm^2/Vs at $T = 100$ mK for samples 1 and 2, respectively. A plot of μ versus T up to 6 K is shown in Fig. 2(b) for samples 1 and 2 and illustrates that the carrier mobility is enhanced as the temperature is decreased and the sample quality is increased (sample 2 has a higher quality, as indicated by its RRR, than sample 1). As shown in Fig. 1(a), a maximum of $\rho_{x,x}$ is obtained at $\mu_0 H^{\mathrm{LT}}_{\rho,\max} \simeq 30$ T, i.e., inside the hidden-order phase, for all the samples. At $T = 1.4$ K, $\rho_{x,x}$ of sample 2 reaches $\simeq$500 $\mu\Omega$ cm at $H^{\mathrm{LT}}_{\rho,\max}$, which is twice the value of $\rho_{x,x}(H^{\mathrm{LT}}_{\rho,\max})$ of sample 1 ($\simeq$300 $\mu\Omega$ cm) and five times that of the third sample studied by Levallois *et al.* ($\simeq$100 $\mu\Omega$ cm) [32]. At $T = 100$ mK, $\rho_{x,x}(H^{\mathrm{LT}}_{\rho,\max})$ of sample 1 increases slightly compared to its value at 1.4 K, while $\rho_{x,x}(H^{\mathrm{LT}}_{\rho,\max})$ of sample 2 increases significantly, reaching $\simeq$650 $\mu\Omega$ cm. The maximum at $H^{\mathrm{LT}}_{\rho,\max}$ indicates a crossover within the hidden-order phase between a low-field Fermi surface with a high carrier mobility to a high-field Fermi surface with a low carrier mobility. The higher the RRR, the higher is $\rho_{x,x}(H^{\mathrm{LT}}_{\rho,\max})$, confirming that the transverse resistivity in the hidden-order phase and its broad maximum at 30 T are dominated by an orbital contribution, i.e., the field-induced cyclotron motion of the charge carriers [17].

Figure 2(c) presents in a log-log scale a Kohler plot, i.e., a plot of $\Delta\rho_{x,x}/\rho^n_{x,x}(H=0)$ versus $[\mu_0 H/\rho^n_{x,x}(H=0)]^2$, for sample 2 at temperatures from 100 mK to 4.2 K. The raw magnetoresistivity $\rho_{x,x}$ versus field data used for the Kohler plot are shown in the Inset of Fig. 2(c). In the Kohler plot, all data sets fall on a single curve, whose field-dependence is close to $\propto H^2$, at fields smaller than 20 T, indicating that a single relaxation time τ can describe the different bands responsible for the high magnetoresistivity [55,56]. Above 20 T, deviations due to Fermi surface reconstructions are observed. Figure 2(d) shows that a plot of the mobility μ, extracted here at different temperatures for samples 1 and 2, versus $1/\rho^n_{x,x}(H=0)$ coincides with a linear function independent of the sample quality. This indicates that the sample and temperature dependencies of the relaxation time τ drive those of both μ and $\rho^n_{x,x}(H=0)$, with a relationship $\mu = a/\rho^n_{x,x}(H=0) = b\tau$, where a and b are constants independent of the temperature and of the sample quality. Despite the complex multiband structure of the Fermi surface of URu_2Si_2 [41,44–47], its transverse magnetoresistivity in high fields $\mathbf{H} \parallel \mathbf{c}$ can thus be rather well described, in a first approximation, by a simple compensated electron-hole two-band picture where the average mobility and the zero-field resistivity are simply controlled by a unique relaxation time τ.

Figure 1(a) also shows that the resistivity $\rho_{x,x}(H)$ of sample 1 exhibits an inflexion point followed by a sudden increase of slope at $\mu_0 H^* = 24.7 \pm 0.5$ T at $T = 100$ mK and $\mu_0 H^* = 24.6 \pm 0.8$ T at $T = 1.4$ K, i.e., well below $H^{\mathrm{LT}}_{\rho,\max}$. For sample 2 at $T = 1.4$ K, such wavelike anomaly is not observed in $\rho_{x,x}(H)$ at fields smaller than $H^{\mathrm{LT}}_{\rho,\max}$ and H^* cannot be defined. In Sec. IV, $\mu_0 H^* \simeq 20$ T is extrapolated for sample 2 in $\mathbf{H} \parallel \mathbf{c}$ from transverse resistivity measurements in a field rotating

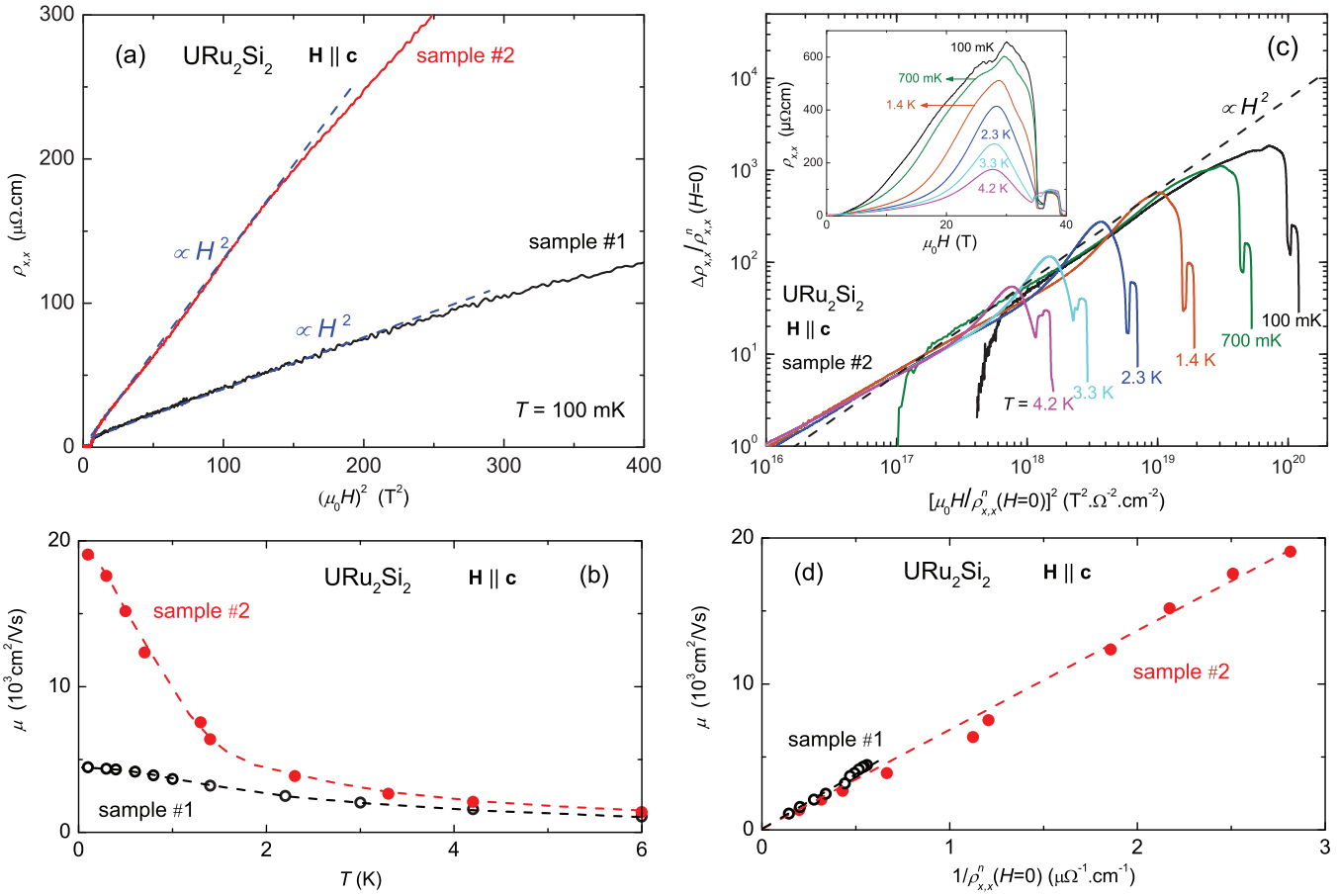

FIG. 2. (Color online) (a) Plot of the transverse resistivity $\rho_{x,x}$ vs H^2, for $\mu_0 H < 20$ T, for samples 1 and 2 at $T = 100$ mK. (b) Plot of the mobility μ vs T for samples 1 and 2 at 100 mK $\leqslant T \leqslant$ 1.4 K. (c) Kohler plot of $\Delta\rho_{x,x}/\rho^n_{x,x}(H = 0)$ vs $[\mu_0 H/\rho^n_{x,x}(H = 0)]^2$ in a log-log scale for sample 2 at temperatures from 100 mK to 4.2 K. (d) Plot of the mobility μ vs $1/\rho^n_{x,x}(H = 0)$ for samples 1 and 2 at 100 mK $\leqslant T \leqslant$ 1.4 K. The dashed lines are guides to the eyes.

from c to a. Another kink developing at around 27 T in the resistivity of sample 2 at $T = 100$ mK may be related to a low-frequency quantum oscillation. For $\mathbf{H} \parallel \mathbf{c}$, an anomaly in the resistivity or Hall effect similar to that observed in the resistivity of sample 1 at $\mu_0 H^* \approx 25$ T was observed at subkelvin temperatures by Shishido *et al.* [48], Altarawneh *et al.* [42], and Aoki *et al.* [43] at $\mu_0 H^* \simeq 22.5$, 24, and 24 T, respectively, but not by Levallois *et al.* [32] at $T = 1.4$ K. In Refs. [42,43,48], the anomaly at H^* has been further related to a field-induced Fermi surface modification, as revealed by changes of the Shubnikov-de Haas frequencies. In Sec. V, we discuss the relationship between H^* and $H^{\mathrm{LT}}_{\rho,\mathrm{max}}$ to field-induced Fermi surface modifications.

IV. ANGULAR DEPENDENCE OF THE HIGH-FIELD RESISTIVITY

URu_2Si_2 exhibits highly anisotropic bulk properties related to its crystal structure. For instance, the in-plane resistivity $\rho_{x,x}(T)$ is twice bigger than the out-of-plane resistivity $\rho_{z,z}(T)$ [8], the superconducting critical field $\mu_0 H_{c,2}$ reaches $\simeq$2–3 T for $\mathbf{H} \parallel \mathbf{c}$ and $\simeq$10–13 T for $\mathbf{H} \parallel \mathbf{a}$ [9,10,57], and the hidden-order phase is destabilized at 35 T for $\mathbf{H} \parallel \mathbf{c}$, while no field-induced transition is observed up to 81 T for $\mathbf{H} \parallel \mathbf{a}$ (see Sec. V). Sugiyama *et al.* [28] and Jo *et al.* [29] have shown, by measuring the magnetization and the resistivity, respectively, that H_1, H_2, and H_3 all follow a $1/\cos\theta$ law, where θ is the angle between **c** and **a**. Shishido *et al.* [48] and Aoki *et al.* [43] observed that the crossover field H^* in the resistivity is governed by a $1/\cos\theta$ law as well. In Ref. [30], we have shown that the field $H^{\mathrm{LT}}_{\rho,\mathrm{max}}$ at the maximum of $\rho_{x,x}(H)$ also follows a $1/\cos\theta$ law. We extend here the study of the angle dependence of the high-field resistivity of URu_2Si_2 by a systematic investigation of $\rho_{x,x}(H)$ for $\mu_0 H$ up to 60 T applied in the three main planes (i) (**c**,**a**) with $\mathbf{a} \parallel \mathbf{I},\mathbf{U}$, (ii) (**c**,**a**) with $\mathbf{a} \perp \mathbf{I},\mathbf{U}$, and (iii) (**a**,**a**). Our two samples 1 and 2 have been characterized in rotating fields.

Figure 3(a) shows the resistivity of sample 2 at $T \simeq 1.5$ K for different angles θ_1 between the magnetic field **H** and the **c** axis. The magnetic field is turning from the transverse ($\mathbf{H} \parallel \mathbf{c}$; $\mathbf{H} \perp \mathbf{I},\mathbf{U}$; $\theta_1 = 0°$) to the longitudinal ($\mathbf{H} \parallel \mathbf{a}$; $\mathbf{H} \parallel \mathbf{I},\mathbf{U}$; $\theta_1 = 90°$) configurations, as illustrated by insets to the graphs. When θ_1 increases, the general form of the resistivity remains unchanged, but the anomalies are shifted to higher field values. The maximal value of $\rho_{x,x}$ at $H^{\mathrm{LT}}_{\rho,\mathrm{max}}$ is also slightly increasing with θ_1. Figure 3(b) shows the resistivity of sample 2 for different angles θ_2 between **H** and **c**, where **H** lies in the (**a**,**c**) plane perpendicular to the electric current, and rotates from

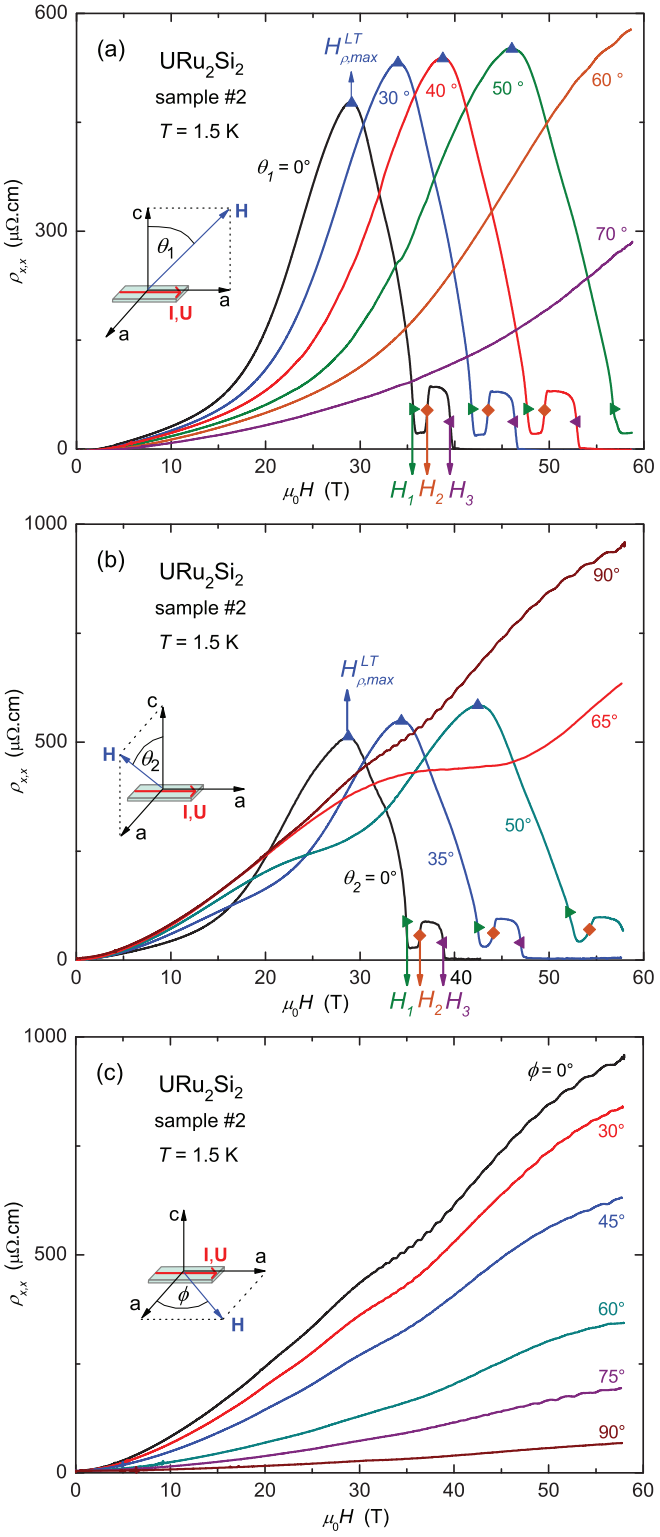

FIG. 3. (Color online) (a) Resistivity $\rho_{x,x}$ vs H of sample 2 at $T = 1.5$ K for different angles θ_1 between **H** and **c**. The field is turning from the transverse ($\theta_1 = 0$) to the longitudinal ($\theta_1 = 90°$) configurations. (b) Resistivity $\rho_{x,x}$ vs H of sample 2 at $T = 1.6$ K for different angles θ_2 between **H** and **c**. The magnetic field is turning in the transverse plane. (c) Resistivity $\rho_{x,x}$ vs H of sample 2 at $T = 1.5$ K for different angles ϕ between **H** and **a**. The field is turning in the (**a**,**a**) plane from the transverse ($\phi = 0$) to the longitudinal ($\phi = 90°$) configurations.

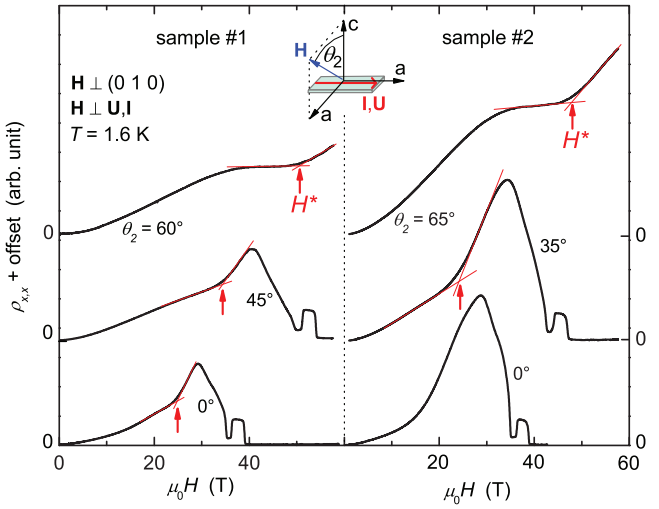

FIG. 4. (Color online) Focus on the anomaly at H^* in the resistivity of samples 1 and 2 for different orientations of **H** in the transverse (**a**,**c**) plane.

the (**H** ∥ **c**; **H** ⊥ **I**,**U**; $\theta_2 = 0°$) to the (**H** ∥ **a**; **H** ⊥ **I**,**U**; $\theta_2 = 90°$) transverse configurations. Again, the fields H_1, H_2, H_3, and $H^{\rm LT}_{\rho,\rm max}$ shift to higher field values with increasing angle θ_2. Remarkably, the heights of the plateaus between H_1 and H_3 are independent of the orientation of the magnetic field relatively to the **c**-axis or to the current [cf. Figs. 3(a) and 3(b)] and of the sample quality (see Fig. 1). In Figure 1(a) (see Sec. III), a kink was observed at $\mu_0 H^* = 25$ T in the resistivity of sample 1, but not in the resistivity of sample 2, for **H** ∥ **c**. In the transverse-to-transverse rotation configuration [see Figs. 3(b) and 4], the anomaly at H^* is unveiled in sample 2 for $\theta_2 \geqslant 35°$, showing a θ_2 dependence similar than that of the anomaly at H^* in sample 1. For $\theta_2 = 90°$, i.e., for **H** ∥ **a**, the transverse resistivity increases continuously up to the highest applied field and no field-induced transition or crossover is observed. Quantum oscillations, whose analysis is given in Sec. V, are discernible in the high-field magnetoresistivity.

Figure 5 shows the angle-dependence of the transition fields H_1, H_2, and H_3, and the crossover fields $H^{\rm LT}_{\rho,\rm max}$ and H^*. Slight misalignments of the samples in the magnetic field are responsible for small differences between the plots in the (a) and (b) panels, which correspond to the transverse-to-longitudinal [Fig. 3(a)] and transverse-to-transverse [Fig. 3(b)] configurations, respectively. The transition fields H_1, H_2 and H_3 are related to the f-electron magnetic properties and all follow a $1/\cos\theta$ law. Their angle-dependence is a direct consequence of the strong Ising-character of the magnetic anisotropy. For both samples 1 and 2, the crossover fields $H^{\rm LT}_{\rho,\rm max}$ and H^* related to Fermi surface modifications (cf. Sec. V) show the same $1/\cos\theta$ dependence as that of the magnetic transition fields. These Fermi surface modifications are thus controlled by the projection of the field along the easy magnetic axis **c**, which illustrates the interplay between the component of the magnetization along **c** and the Fermi surface in URu_2Si_2. A fit by a $1/\cos\theta$ law allows extracting $\mu_0 H^* \simeq 20$ T for sample 2 in the limit of $\theta_2 \simeq 0°$, i.e., for **H** ∥ **c**. $\mu_0 H^*$ in sample 2 is much smaller than the values of 25 T found for sample 1 and those between 22.5 and 24 T reported in

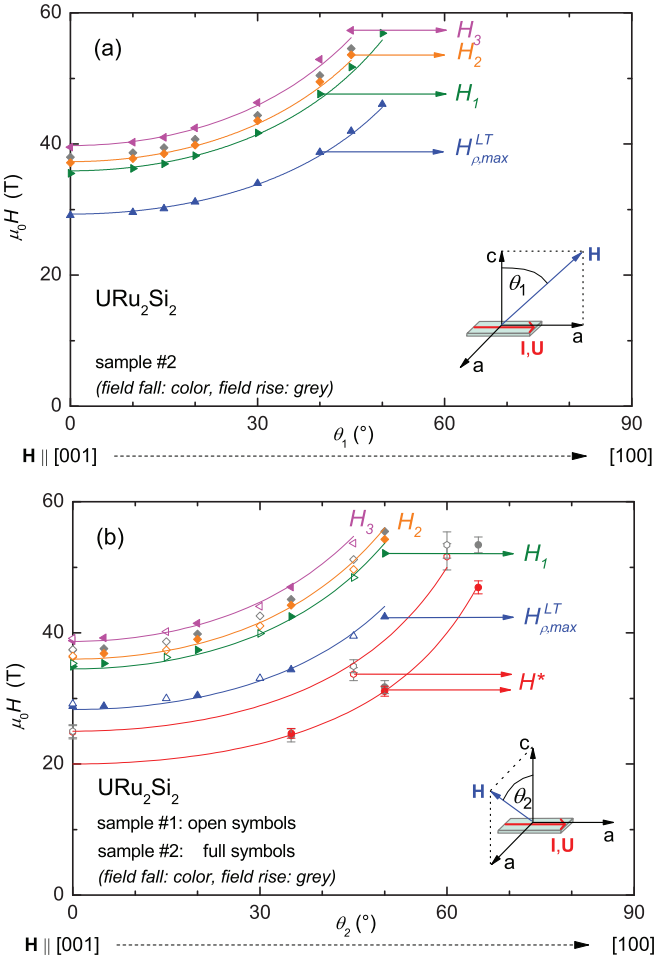

FIG. 5. (Color online) Angle dependence of the transition fields H_1, H_2, and H_3 and crossover fields $H^{\rm LT}_{\rho,\rm max}$ and H^* of sample 1 (open symbols) and sample 2 (closed symbols). Data from the rise of the pulse are in grey, data from the fall of the pulse are in color. The solid lines represent $1/\cos\theta$ fits to the data.

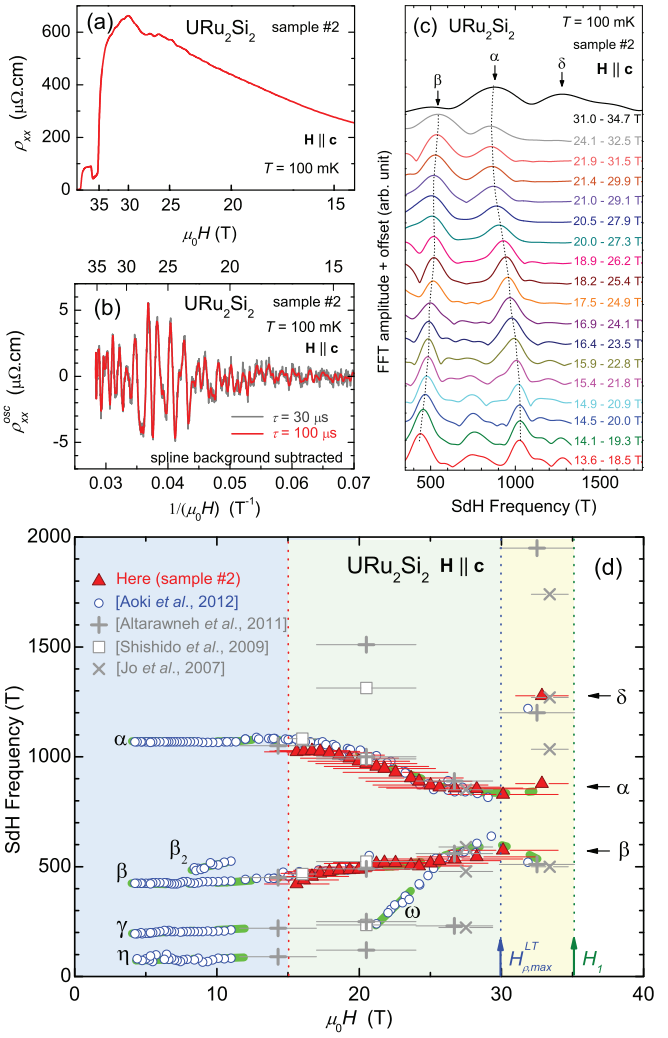

FIG. 6. (Color online) (a) Resistivity $\rho_{x,x}$ of sample 2 at $T = 100$ mK in $\mathbf{H} \parallel \mathbf{c}$. (b) Oscillating signal extracted using a spline background, with the time constants $\tau = 30$ and 100 μs (digital lock-in). (c) Fourier transform spectra for a large set of small field windows. (d) Field dependence of the Shubnikov-de Haas frequencies extracted here (pulsed fields) and compiled from Refs. [29,42,43,48] (steady fields). The horizontal bars indicate the field windows of the Fourier transform and the dotted lines are guides to the eyes.

the literature [42,43,48]. For $\mathbf{H} \parallel \mathbf{c}$, the anomaly at H^* in the resistivity of sample 2 might be hidden by an additional orbital contribution whose intensity decreases at high θ_2 angles.

Figure 3(c) shows the resistivity of URu_2Si_2 for different directions of the magnetic field inside the (**a**,**a**) plane, ϕ being the angle between the magnetic field **H** and the **a**-axis. The transverse ($\phi = 0°$) to longitudinal ($\phi = 90°$) configurations are explored. The curves show Shubnikov-de Haas quantum oscillations, which are analyzed in Sec. V. The resistivity decreases with increasing angle ϕ and the field-dependent term vanishes almost totally at 90°. In Ref. [17], we have shown that the strong field-induced transverse resistivity $\rho_{xx}(H)$, which develops below T_0 for $\mathbf{H} \parallel \mathbf{a}$, is characteristic of the hidden-order phase. The fact that this contribution vanishes in the longitudinal configuration for $\mathbf{H} \parallel \mathbf{a} \parallel \mathbf{I},\mathbf{U}$, confirms the orbital origin of $\rho_{x,x}$ for $\mathbf{H} \parallel \mathbf{a} \perp \mathbf{I},\mathbf{U}$.

V. HIGH-FIELD FERMI SURFACE

A. Quantum oscillations for H ∥ c

Figure 6(a) shows the resistivity $\rho_{x,x}$ of sample 2 at $T = 100$ mK in a pulsed magnetic field $\mathbf{H} \parallel \mathbf{c}$, and Figure 6(b) shows the oscillating signal extracted by subtracting a spline background from the raw resistivity. To get a better sensibility, Fourier transforms were made on data extracted using a digital lock-in with a small time constant $\tau = 30$ μs. For clarity, oscillating data extracted using a higher time constant $\tau = 100$ μs are shown in Fig. 6(b) too. Shubnikov-de Haas oscillations are observed here from 15 T to $\mu_0 H_1 = 35$ T. The corresponding Fourier spectra are shown in Fig. 6(c) for a large set of small field windows [58]. Figure 6(d) presents the field dependence of the Shubnikov-de Haas frequencies. In all explored field windows between 15 to 30 T, the frequencies F_β and F_α, which at low field equal $\simeq$400 and $\simeq$1000 T, respectively, are observed. A progressive frequency change, signature of a continuous Fermi surface modification, occurs within a large field window going from 15 to 30 T, where F_β increases, while F_α decreases as

H increases. The sample-dependent crossover field $\mu_0 H^* \simeq$ 20–25 T lies in this field window and could possibly be a signature of the associated Fermi surface change. A sudden spectrum modification occurs at $\mu_0 H^{\rm LT}_{\rho,\rm max} = 30$ T, at which the frequency F_α reaches $\simeq$850 T, and above which the Fermi surface is reconstructed: for $\mu_0 H^{\rm LT}_\rho < \mu_0 H < \mu_0 H_1 = 35$ T, F_α remains almost field-independent, we loose the trace of F_β, and a new frequency $F_\delta \simeq 1300$ T appears. For comparison, the frequencies extracted from studies in steady magnetic fields [29,42,43,48] are also plotted in Fig. 6(d). An excellent agreement is found between our data and that from Aoki *et al.* [43], where a similar analysis as here, i.e., with a high number of small field windows, was carried out. Due to the electronic noise of our pulsed field experiment, we were not able to observe here the low frequencies η, γ, and ω found by Aoki *et al.* [43]. Surprisingly, we were able to follow the β frequency from 22 to 25 T, even though Aoki *et al.* [43] did not observed it. Our data are also in good agreement with that from Altarawneh *et al.* [42], Jo *et al.* [29], and Shishido *et al.* [48], where Fourier transforms were done on fewer field windows. However, a high frequency of $\simeq$1500 T was extracted at $\simeq$20 T by Altarawneh *et al.* [42] but not here nor by Aoki *et al.* [43]. As well, we found no trace of the frequency $F_\varepsilon \simeq 1300$ T reported by Shishido *et al.* [48] above $\mu_0 H = 20T$. In the window 25–30 T, Altarawneh *et al.* [42] and Jo *et al.* [29] extracted a low frequency of $\simeq$250 T, which was not observed here nor by Aoki *et al.* [43]. As well, in the window 30–35 T, Altarawneh *et al.* [42] and Jo *et al.* [29] found a high frequency of $\simeq$1500–2000 T, which was not observed here nor by Aoki *et al.* [43]. The differences between these studies come from the difficulty to extract fine Fourier transform spectra in field windows smaller than a few Shubnikov-de Haas periods. Another difficulty is that the observed frequencies result from the sum or subtraction of harmonic frequencies to the fundamental frequencies, which prevents from extracting real fundamental frequencies. Despite these difficulties, all experimental studies agree on the fact that a magnetic field applied along **c** induces successive modifications of the Fermi surface in magnetic fields far below $\mu_0 H_1 = 35$ T, i.e., in the hidden-order phase.

B. Quantum oscillations for H ⊥ c

Figure 7(a) shows the transverse resistivity $\rho_{x,x}$ of sample 2 as function of **H** applied along the **a**-axis, at temperatures from 500 mK to 4.2 K. At $T = 500$ mK, the sample is superconducting up to $\mu_0 H_{c,2} \simeq 9$ T [defined at a kink in $\rho_{x,x}(H)$], above which $\rho_{x,x}$ increases significantly with H, from $\simeq$50 $\mu\Omega$cm at 10 T to 1150 $\mu\Omega$cm at 55 T. No field-induced transition is observed in our resistivity data at $T = 1.5$ K and the system remains in the hidden-order phase up to 81 T. This agrees well with the report by Yanagisawa *et al.* [19] of a lack of anomaly in the elastic constant in $\mu_0 \mathbf{H} \parallel \mathbf{a}$ up to 69 T, at $T = 1.5$ K. At $T = 500$ mK and above $H_{c,2}$, the nonoscillating part of $\rho_{x,x}$ is almost linear and clearly deviates from the H^2 law expected in a one-band Fermi liquid picture. Slow and fast Shubnikov-de Haas oscillations are visible in the raw data up to the highest investigated fields. No change of the SdH frequencies as function of the magnetic field is observed within our experimental resolution, which

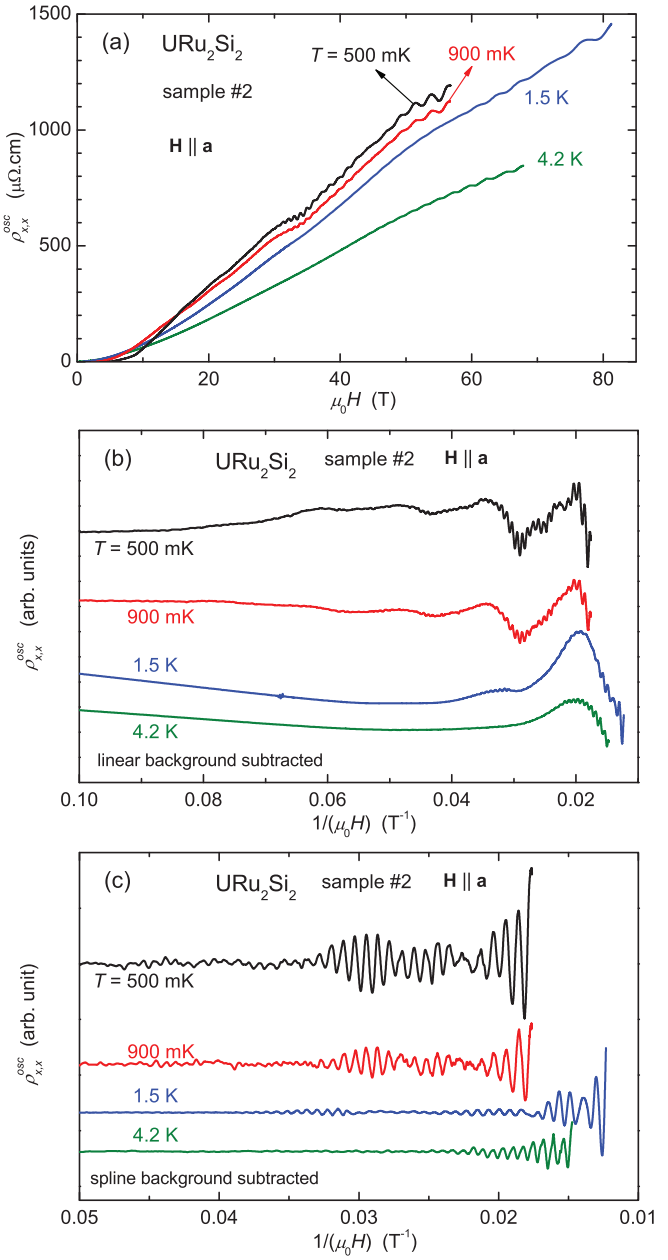

FIG. 7. (Color online) For sample 2 in $\mathbf{H} \parallel \mathbf{a}$. (a) Transverse resistivity $\rho_{x,x}$ vs H, at 500 mK $\leqslant T \leqslant$ 4.2 K. (b) Oscillating resistivity $\rho^{\rm osc}_{x,x}$ extracted using a linear background vs $1/H$. (c) Fast oscillating resistivity extracted using a spline background.

indicates that the Fermi surface remains unchanged in a high magnetic field up to 81 T applied along **a**. The slow oscillations shown in Fig. 7(b) were extracted using linear backgrounds. Figure 8(a) shows the corresponding Fourier spectra, which exhibit peaks at $F_\gamma = 70$ T, at its harmonics $F_{2\gamma} = 140$ T and $F_{3\gamma} = 210$ T, and at $F_\alpha = 1185$ T, in good agreement with previous low-field reports [40,41]. The fast oscillating signal shown in Fig. 7(c) was extracted using a spline background. The corresponding spectra are shown in Fig. 8(b): in addition to the main peak at $F_\alpha = 1185$ T, a shoulder is attributed to a peak at $F_\lambda \simeq 1350$ T. While the intensity of α vanishes rapidly with T due to the high effective mass $m^*_\alpha = 9.7 m_0$ [43],

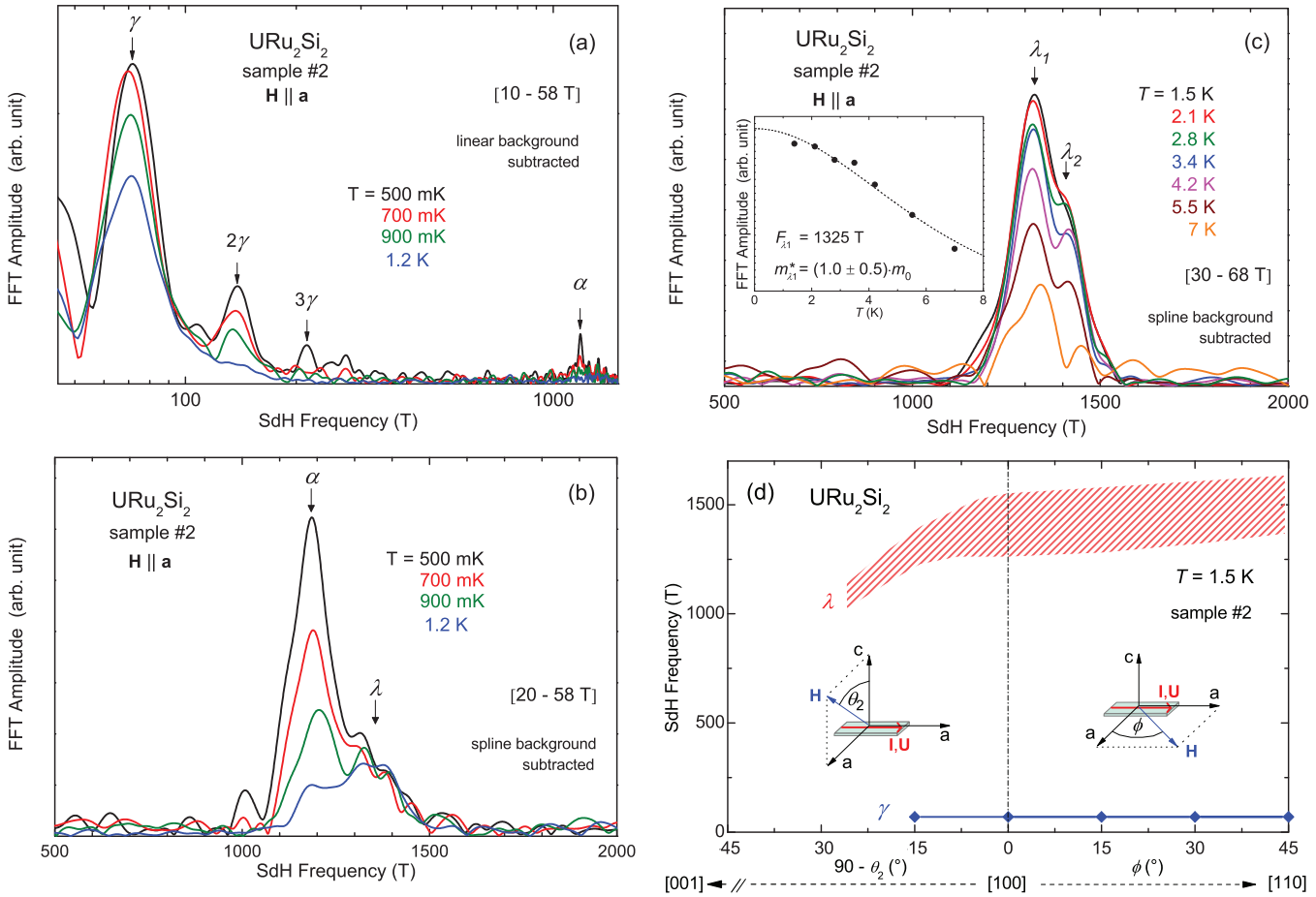

FIG. 8. (Color online) For sample 2 in **H** ∥ **a**. (a) Fourier spectra of the oscillations extracted using linear backgrounds at 500 mK ⩽ T ⩽ 1.2 K. (b) Spectra of the fast SdH oscillations extracted using spline backgrounds at 500 mK ⩽ T ⩽ 1.2 K. (c) Spectra of the fast SdH oscillations extracted using spline backgrounds at 1.5 K ⩽ T ⩽ 10 K. (Inset) Plot of the amplitude of λ_1 vs T and fit of the related mass using the Lifshitz-Kosevich formula. (d) Angular dependence of the SdH frequencies F_γ and F_λ observed here at T =1.5 K. For the λ branch, the shaded area indicates the frequency ranges at which the Fourier spectra are enhanced in (c).

the intensity of λ decreases much slower with T. Figure 8(c) shows, for 1.4 ⩽ T ⩽ 10 K, the spectra of sample 2 extracted using spline backgrounds. For T ⩾ 1.4 K, a higher excitation current allowed to reach a better sensitivity than at subkelvin temperatures (where high excitation currents are prohibited). The spectra show that α has almost totally vanished above 1.5 K and that λ survives up to more than 7 K, being split into two frequencies $F_{\lambda_1} \simeq 1325$ T and $F_{\lambda_2} \simeq 1400$ T. The effective mass $m^*_{\lambda_1} = (1.0 \pm 0.5)m_0$ deduced from the temperature dependence of the λ_1 amplitude is a factor 10 smaller than the effective mass of α [43]. Alternatively, the frequency F_λ could result from the combination of other frequencies (F_α, F_γ, etc.) but, within such scenario, the mass of λ should be heavier than the masses of the original and uncombined frequencies. In Appendix, further evidences supporting the observation of the new λ branch are given, and we show that slight misalignments of the sample in a field **H** ∥ **a** modify its splitting, which is very sensitive to the field direction. Figure 8(d) presents the angle dependence of the Shubnikov-de Haas frequencies of the γ and λ branches extracted from resistivity measurements in a field applied in the (**a**,**c**) and (**a**,**a**) planes (cf. Fig. 3). A slight increase by ∼50 T of F_λ is observed as the field-direction moves from [100] ($\phi = 0°$) to [110] ($\phi = 45°$). When the field rotates from [100] ($\theta_2 = 90°$) to [001] ($\theta_2 = 0°$), F_λ decreases more significantly, from ∼1350 T at $\theta_2 = 90°$ to ∼1100 T at $\theta_2 = 60°$, and its trace is lost at angles $\theta_2 < 60°$. The angle dependence of the λ frequencies, which are observed here in the (**a**,**a**) plane, and out of the (**a**,**a**) plane [at angles $(90 - \theta_2)$ up to 30°], is compatible with a large and almost spherical Fermi surface similar to the α branch. In agreement with previous reports (see Ref. [43]), no variation of F_γ is observed for the investigated field directions.

VI. DISCUSSION

High-quality URu_2Si_2 samples exhibit a remarkably strong magnetoresistivity inside the hidden-order phase, which is dominated by the orbital effect, as shown by the sample and angle dependencies of the resistivity. The resistivity of our highest-quality sample increases by three orders of magnitude as a magnetic field applied along the **a** axis increases from the low-field range (in the normal state) to 81 T. The high quality of our samples and the high carrier mobility [31] are responsible for this exceptionally large orbital effect.

The angle-dependent study of the resistivity shows that the magnetic transitions and the electronic anomalies related to the Fermi surface changes exhibit the same angle dependence in $1/\cos\theta$, where θ is the angle between **H** and **c**, indicating the strong correlation between the Fermi surface and the magnetic polarization induced along the **c** axis in URu_2Si_2. A magnetic field applied along the easy magnetic axis **c** destabilizes the hidden-order phase at $\mu_0 H_1 = 35$ T, but no anomaly is induced when the magnetic field is applied along the hard axis **a**, at least up to 81 T. At zero magnetic field, the hidden-order phase is thus stabilized by the strong Ising-character of the magnetic properties. At $T = 1.4$ K, for $H > H_1$ applied along the **c** axis, the resistivity is neither sample-dependent nor angle-dependent and has no observable orbital contribution. However, a peculiar sample dependence of the resistivity in the regime $H_1 < H < H_3$ develops at $T = 100$ mK, indicating an interplay between the orbital motion of the electrons and the magnetic properties. As observed in the magnetization $M(H)$ (cf. Refs. [14,15,17]) successive partial polarizations of the 5*f*-electron moments occur at H_1, H_2, and H_3. Observations by Nernst, Hall, and Shubnikov-de Haas effects (cf. Refs. [32,42]) indicate that these polarizations induce Fermi surface reconstructions, due to reconstructions of the magnetic Brillouin zone, at H_1, H_2, and H_3. We have shown that a magnetic field applied along the **c** axis induces anomalies in the orbital contribution to the resistivity at $\mu_0 H^* \simeq 20$–25 T and $\mu_0 H^{\rm LT}_{\rho,\rm max} \simeq 30$ T, i.e., at fields well below the destruction of the hidden-order phase at $\mu_0 H_1 = 35$ T. In the literature, similar anomalies were observed at $\mu_0 H^* \simeq 23$–25 T not only in the resistivity of other samples [42,43,48] but also in Hall resistivity [24,48] and thermopower [24,25] data. A change of slope of $\rho_{x,x}(H)$ at $\simeq$8 T is related to a splitting of the β branch in Refs. [41,43]. In the thermoelectric power, local maxima at $\simeq$24 and $\simeq$30 T were attributed to the signatures of Lifshitz-transitions [24,25]. The evolution of the Shubnikov-de Haas spectra clearly indicates field-induced Fermi surface reconstructions inside the hidden-order phase. In particular, a Fermi surface reconstruction occurs at $\mu_0 H^{\rm LT}_{\rho,\rm max} = 30$ T, at which the resistivity is maximum. We note that the low-temperature magnetization shows no anomaly in the field range 0–35 T (cf. Refs. [15,17]). The observed anomalies in the transport properties are thus due to Fermi surface instabilities. The hidden-order parameter and field-induced polarization of the 5*f*-electron magnetic moments are in strong competition, which results in the transition at $\mu_0 H_1 = 35$ T for $\mathbf{H} \parallel \mathbf{c}$. In Ref. [17], we have shown that the onset of intersite electronic interactions, presumably antiferromagnetic fluctuations, is a precursor of the hidden-order phase. Modeling the interplay between the evolutions of the Fermi surface and the hidden-order and their relation with the magnetic anisotropy is expected to be a key for describing URu_2Si_2.

A new Fermi surface sheet of frequency $F_\lambda \simeq 1350$ T and effective mass $m^*_\lambda \simeq (1 \pm 0.5) m_0$ for $\mathbf{H} \parallel \mathbf{a}$ has been observed here by high-field magnetoresistivity experiments. Using the formula, approximated for a spherical Fermi surface, of the Sommerfeld coefficient $\gamma = \sum_i \gamma_i \approx \sum_i k_B^2 V m^*_i k_{Fi}/(3\hbar^2)$, where $V = 49$ cm^3/mol is the molar volume, $k_{Fi} = \sqrt{2eF_i/\hbar}$ is the wave vector, F_i is the SdH frequency, and γ_i is the contribution to the Sommerfeld coefficient from the Fermi sheet i [41], we estimate the contribution of the new band λ by $\gamma_\lambda \simeq 0.5$ mJ/mol K^2, which represents less than 1% of the Sommerfeld coefficient $\gamma_{Cp} \simeq 65$ mJ/mol K^2 extracted from the specific heat [4]. Recent cyclotron resonance experiments [46,47] permitted to report new Fermi surface branches, which had not yet been observed by quantum oscillation techniques. One of these new branches κ was found to be particularly heavy, weighting as 30% of γ_{Cp}. The new branch λ observed here could possibly correspond to one of the four other new and light branches (noted F, G, H, and I) observed by cyclotron resonance in Refs. [46,47]. We note that band calculation models, as those developed in Refs. [44,45], might be refined to present the new light band λ observed here.

VII. CONCLUSION

We have performed a systematic investigation of the high-field resistivity of URu_2Si_2 high-quality single crystals in pulsed magnetic fields up to 81 T. As shown by a Kohler plot and by a simple relationship $\mu \propto 1/\rho^n_{x,x}(H = 0)$ between the carrier mobility for $\mathbf{H} \parallel \mathbf{c}$ and the zero-field resistivity (in the normal state), the nonoscillating low-field magnetoresistivity can be described using a unique relaxation time τ for all contributing bands. For $\mathbf{H} \parallel \mathbf{c}$, crossovers associated with a kink in $\rho_{x,x}(H)$ at $\mu_0 H^* = 20$–25 T and with a maximum of $\rho_{x,x}(H)$ at $\mu_0 H^{\rm LT}_{\rho,\rm max} = 30$ T are related to Fermi surface modifications within the hidden-order phase. While $H^{\rm LT}_{\rho,\rm max}$ is almost sample-independent, we find out that H^* is strongly sample-dependent and can be hidden in high-quality crystals where a huge orbital effect contributes to $\rho_{x,x}$. We have established that the low-temperature phase transitions H_1, H_2, H_3 and crossovers H^* and $H^{\rm LT}_{\rho,\rm max}$ are controlled by a $1/\cos\theta$ law, where θ is the angle between **H** and the **c** axis. For $\mu_0 \mathbf{H} \parallel \mathbf{a}$ up to 81 T, the system remains in its hidden-order state and no Fermi surface change is observed. In this field configuration, quantum oscillations from a new and possibly spherical branch λ of frequency $F_\lambda \simeq 1350$ T and effective mass $m^*_\lambda \simeq (1 \pm 0.5)\, m_0$ are observed up to 7 K. As well as the α branch, the λ branch is found to be split. The work presented here, as an extension to lower temperatures, higher fields, and new field configurations of our work published in Ref. [17] strongly supports that the interplay between the Fermi surface, the magnetic properties, and the hidden-order plays a significant role in URu_2Si_2. This should be considered for the development of realistic models describing the hidden-order state in URu_2Si_2.

ACKNOWLEDGMENTS

We acknowledge K. Behnia, J.-P. Brison, M. Goiran, H. Harima, and J. Levallois for useful discussions, X. Fabrèges for the development of a numerical lock-in, and L. Bendichou, P. Delescluse, T. Domps, J-M. Lagarrigue, J.-P. Nicolin, C. Proust, and T. Schiavo for technical support. This work was supported by Euromagnet II via the EU under Contract No. RII3-CT-2004-506239 and by the ERC Starting Grant NewHeavyFermion.

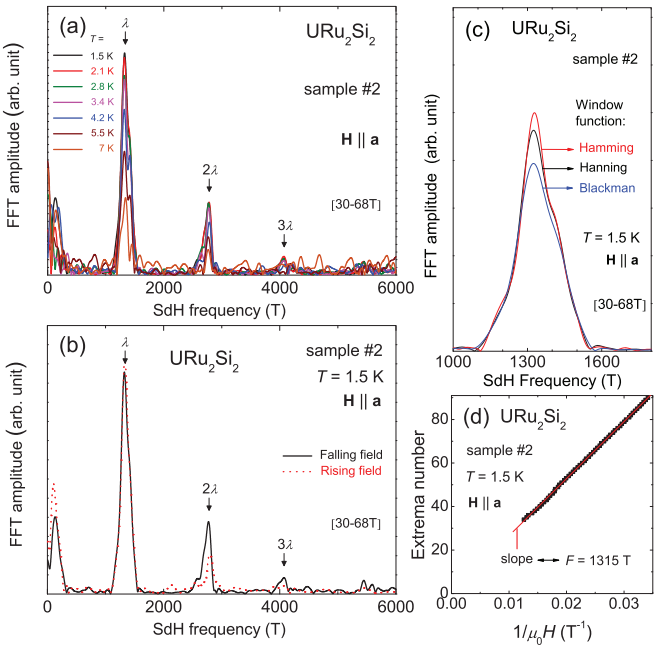

FIG. 9. (Color online) For URu_2Si_2 sample 2 in a field $\mathbf{H} \parallel \mathbf{a}$. (a) Fourier spectra at frequencies up to 6000 T of the oscillations extracted (a) at $1.5 \leqslant T \leqslant 7$ K (falling field) and (b) at $T = 1.5$ K for falling and rising field, (c) Fourier spectra at $T = 1.5$ K made using Hanning, Hamming, and Blackman window functions, and (d) Onsager plot of the extrema number vs $1/\mu_0 H$ for the quantum oscillations at the frequency F_λ, at $T = 1.5$ K.

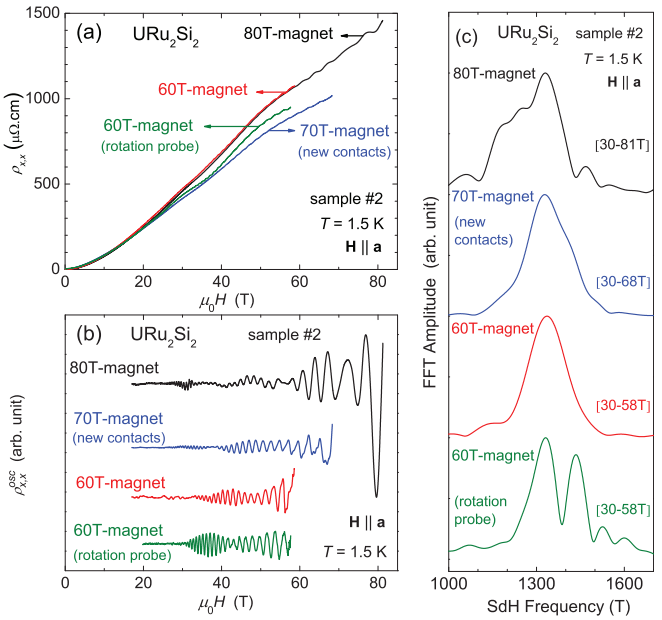

FIG. 10. (Color online) (a) Transverse magnetoresistivity $\rho_{x,x}$ vs magnetic field H applied along the **a** axis of sample 2 at $T = 1.5$ K. Comparison of measurements in different cryostat-coil setups, from different sets of measurements. Corresponding (b) oscillating signals $\rho^{\rm osc}_{x,x}(H)$ and (c) Fourier transforms.

APPENDIX

Here, we presents further elements supporting the observation of a new orbit λ at the frequency $F_\lambda \simeq 1350$ T, but also indicating some of the experimental limits of the data collected for $\mathbf{H} \parallel \mathbf{a}$. Figure 9(a) shows that harmonics of λ up to the third degree are observed at temperatures from $T = 1.5$ to 7 K (experiment done using a 70-T magnet). Figure 9(b) shows that, at $T = 1.5$ K, these harmonics are observed for both rising and falling parts of the pulsed field. Figure 9(c) shows Fourier transforms of the data made using different window functions (Hanning, Hamming, and Blackman [53]) which lead to very similar spectra. In the present work, a Hanning window has been used to analyze all sets of data. Figure 9(d) shows an Onsager plot, i.e., a plot of the extrema number versus the inverse of the magnetic field, corresponding to the fast oscillations at the frequency F_λ (data obtained using a 80-T magnet). From a linear fit of these data points, we extract a slope 1315 $T^{-1} \simeq F_\lambda$. Figure 10(a) shows different sets of measurements of the magnetoresistivity $\rho_{x,x}$ of sample 2 for $\mathbf{H} \parallel \mathbf{a}$ at $T = 1.5$ K, from experiments carried out with 60-, 70-, and 80-T magnets, with rotating and nonrotating probes. Figure 10(b) shows the corresponding oscillating magnetoresistivity $\rho^{\rm osc}_{x,x}(H)$ and Fig. 10(b) their Fourier transforms. Small variations in the absolute values of $\rho_{x,x}$ as in the oscillating signals $\rho^{\rm osc}_{x,x}$ and their Fourier transforms result from small misalignments of the sample and new electrical contacts (after repair). Limits of reproducibility in our measurements lead to slight differences in the splitting of the λ branch, which is mainly made of two or three satellites. A strong sensitivity with the field direction of the λ branch satellites might be responsible for this effect. Oppositely, when the field is applied along the c axis, the reproducibility of our data was found to be excellent, since the physics is then governed by the projection of the field along **c** (cf. Sec. IV) and is thus almost insensitive to slight misorientations of the sample in the magnetic field.

[1] J. A. Mydosh and P. M. Oppeneer, Rev. Mod. Phys. **83**, 1301 (2011).

[2] T.T.M. Palstra, A.A. Menovsky, J. van den Berg, A.J. Dirkmaat, P.H. Kes, G.J. Nieuwenhuys, and J.A. Mydosh, Phys. Rev. Lett **55**, 2727 (1985).

[3] W. Schlabitz, J. Baumann, B. Pollit, U. Rauchschwalbe, H. M. Mayer, U. Ahlheim, and C. D. Bredl, Z. Phys. B **62**, 171 (1986).

[4] M.B. Maple, J.W. Chen, Y. Dalichaouch, T. Kohara, C. Rossel, M.S. Torikachvili, M.W. McElfresh, and J.D. Thompson, Phys. Rev. Lett. **56**, 185 (1986).

[5] A. P. Ramirez, P. Coleman, P. Chandra, E. Brück, A. A. Menovsky, Z. Fisk, and E. Bucher, Phys. Rev. Lett. **68**, 2680 (1992).

[6] F. Bourdarot, A. Bombardi, P. Burlet, M. Enderle, J. Flouquet, P. Lejay, N. Kernavanois, V. P. Mineev, L. Paolasini, M. E. Zhitomirsky, and B. Fåk, Physica B **359-361**, 986 (2005).

[7] A. LeR. Dawson, W. R. Datars, J. D. Garrett, and F. S. Razavi, J. Phys.: Condens. Matter **1**, 6817 (1989).

[8] T.T.M. Palstra, A.A. Menovsky, and J.A. Mydosh, Phys. Rev. B **33**, 6527 (1986).

[9] H. Ohkuni, T. Ishida, Y. Inada, Y. Hagam E. Yamamoto, Y. Ōnuki, and S. Takahasi, J. Phys. Soc. Jpn. **66**, 4 (1997).

[10] W.K. Kwok, L.E. DeLong, G.W. Crabtree, D.G. Hinks, and R. Joynt, Phys. Rev. B **41**, 11649 (1990).

[11] G. Motoyama, T. Nishioka, and N. K. Sato, Phys. Rev. Lett. **90**, 166402 (2003).

[12] H. Amitsuka, K. Matsuda, I. Kawasaki, K. Tenya, M. Yokoyama, C. Sekine, N. Tateiwa, T. C. Kobayashi, S. Kawarazaki, and H. Yoshizawa, J. Magn. Magn. Mater. **310**, 214 (2007).

[13] E. Hassinger, G. Knebel, K. Izawa, P. Lejay, B. Salce, and J. Flouquet, Phys. Rev. B **77**, 115117 (2008).

[14] A. de Visser, F. R. de Boer, A. A. Menovsky, and J. J. M. Franse, Solid State Commun. **64**, 527 (1986).

[15] K. Sugiyama, M. Nakashima, H. Ohkuni, K. Kindo, Y. Haga, T. Honma, E. Yamamoto, and Y. Ōnuki, J. Phys. Soc. Jpn. **68**, 3394 (1999).

[16] N. Harrison, M. Jaime, and J. A. Mydosh, Phys. Rev. Lett. **90**, 096402 (2003).

[17] G. W. Scheerer, W. Knafo, D. Aoki, G. Ballon, A. Mari, D. Vignolles, and J. Flouquet, Phys. Rev. B **85**, 094402 (2012).

[18] A. Suslov, J. B. Ketterson, D. G. Hinks, D. F. Agterberg, and B. K. Sarma, Phys. Rev. B **68**, 020406 (2003).

[19] T. Yanagisawa, S. Mombetsui, H. Hidaka, H. Amitsuka, M. Akatsu, S. Yasin, S. Zherlitsyn, J. Wosnitza, K. Huang, and M. B. Maple, J. Phys. Soc. Jpn. **82**, 013601 (2013).

[20] T. Yanagisawa, S. Mombetsu, H. Hidaka, H. Amitsuka, M. Akatsu, S. Yasin, S. Zherlitsyn, J. Wosnitza, K. Huang, M. Janoschek, and M. B. Maple, Phys. Rev. B **88**, 195150 (2013).

[21] K. H. Kim, N. Harrison, M. Jaime, G. S. Boebinger, and J. A. Mydosh, Phys. Rev. Lett. **91**, 256401 (2003).

[22] M. Jaime, K.H. Kim, G. Jorge, S. McCall, and J.A. Mydosh, Phys. Rev. Lett. **89**, 287201 (2002).

[23] V. F. Correa, S. Francoual, M. Jaime, N. Harrison, T. P. Murphy, E. C. Palm, S. W. Tozer, A. H. Lacerda, P. A. Sharma, and J. A. Mydosh, Phys. Rev. Lett. **109**, 246405 (2012).

[24] L. Malone, T.D. Matusda, A. Antunes, G. Knebel, V. Taufour, D. Aoki, K. Behnia, C. Proust, and J. Flouquet, Phys. Rev. B **83**, 245117 (2011).

[25] A. Pourret, A. Palacio-Morales, S. Krmer, L. Malone, M. Nardonne, D. Aoki, G. Knebel, and Jacques Flouquet, J. Phys. Soc. Jpn. **82**, 034706 (2013).

[26] K. Kuwahara, S. Yoshii, H. Nojiri, D. Aoki, W. Knafo, F. Duc, X. Fabreges, G.W. Scheerer, P. Frings, G.L.J.A. Rikken, F. Bourdarot, L.P. Regnault, and J. Flouquet, Phys. Rev. Lett. **110**, 216406 (2013).

[27] D. Aoki, W. Knafo, and I. Sheikin, C. R. Phys. **14**, 53 (2013).

[28] K. Sugiyama, H. Fuke, K. Kindo, K. Shimohata, A. A. Menovsky, J. A. Mydosh, and M. Muneyuki Date, J. Phys. Soc. Jpn. **59**, 9 (1990).

[29] Y.J. Jo, L. Balicas, C. Capan, K. Behnia, P. Lejay, J. Flouquet, J.A. Mydosh, and P. Schlottmann, Phys. Rev. Lett. **98**, 166404 (2007).

[30] G. W. Scheerer, W. Knafo, D. Aoki, and J. Flouquet, J. Phys. Soc. Jpn. **81**, SB005 (2012).

[31] Y. Kasahara, T. Iwasawa, H. Shishido, T. Shibauchi, K. Behnia, Y. Haga, T. D. Matsuda, Y. Onuki, M. Sigrist, and Y. Matsuda, Phys. Rev. Let. **99**, 116402 (2007).

[32] J. Levallois, K. Behnia, J. Flouquet, P. Lejay, and C. Proust, Europhys. Lett. **85**, 27003 (2009).

[33] J. Schoenes, C. Schonenberger, J. J. M. Franse, and A. A. Menovsky, Phys. Rev. B **35**, 5375 (1987).

[34] A. F. Santander-Syro, M. Klein, F. L. Boariu, A. Nuber, P. Lejay, and F. Reinert, Nat. Phys. **5**, 637 (2009).

[35] I. Kawasaki, S.I. Fujimori, Y. Takeda, T. Okane, A. Yasui, Y. Saitoh, H. Yamagami, Y. Haga, E. Yamamoto, and Y. Onuki, Phys. Rev. B **83**, 235121 (2011).

[36] R. Yoshida, Y. Nakamura, M. Fukui, Y. Haga, E. Yamamoto, Y. Onuki, M. Okawa, S. Shin, M. Hirai, Y. Muraoka, and T. Yokoya, Phys. Rev. B **82**, 205108 (2010).

[37] R. Bel, H. Jin, K. Behnia, J. Flouquet, and P. Lejay, Phys. Rev. B **70**, 220501(R) (2004).

[38] C. Bergemann, S. R. Julian, G. J. McMullan, B. K. Howard, G. G. Lonzarich, P. Lejay, J. P. Brison, and J. Flouquet, Physica B **230-232**, 348 (1997).

[39] N. Keller, S. A. J. Wiegers, J. A. A. J. Perenboom, A. de Visser, A. A. Menovsky, and J. J. M. Franse, J. Magn. Magn. Mater. **177-181**, 298 (1998).

[40] H. Ohkuni, Y. Inada, Y. Tokiwa, K. Sakurai, R. Settai, T. Honma, Y. Haga, E. Yamamoto, Y. Ōnuki, H. Yamagami, S. Takahashi, and T. Yanagisawa, Philos. Mag. B **79**, 1045 (1999).

[41] E. Hassinger, G. Knebel, T. D. Matsuda, D. Aoki, V. Taufour, and J. Flouquet, Phys. Rev. Lett. **105**, 216409 (2010).

[42] M. M. Altarawneh, N. Harrison, S. E. Sebastian, L. Balicas, P. H. Tobash, J. D. Thompson, F. Ronning, and E. D. Bauer, Phys. Rev. Let. **106**, 146403 (2011).

[43] D. Aoki, G. Knebel, I. Sheikin, E. Hassinger, L. Malone, D. Matsuda, and J. Flouquet, J. Phys. Soc. Jpn. **81**, 074715 (2012).

[44] P. M. Oppeneer, J. Rusz, S. Elgazzar, M.-T. Suzuki, T. Durakiewicz, and J. A. Mydosh, Phys. Rev. B **82**, 205103 (2010).

[45] H. Ikeda, M.-T. Suzuki, R. Arita, T. Takimoto, T. Shibauchi, and Y. Matsuda, Nat. Phys. **8**, 528 (2012).

[46] S. Tonegawa, K. Hashimoto, K. Ikada, Y.-H. Lin, H. Shishido, Y. Haga, T. D. Matsuda, E. Yamamoto, Y. Onuki, H. Ikeda, Y. Matsuda, and T. Shibauchi, Phys. Rev. Lett. **109**, 036401 (2012).

[47] S. Tonegawa, K. Hashimoto, K. Ikada, Y. Tsuruhara, Y.-H. Lin, H. Shishido, Y. Haga, T. D. Matsuda, E. Yamamoto, Y. Onuki, H. Ikeda, Y. Matsuda, and T. Shibauchi, Phys. Rev. B **88**, 245131 (2013).

[48] H. Shishido, K. Hashimoto, T. Shibauchi, T. Sasaki, H. Oizumi, N. Kobayashi, T. Takamasu, K. Takehana, Y. Imanaka, T. D. Matsuda, Y. Haga, Y. Onuki, and Y. Matsuda, Phys. Rev. Lett. **102**, 156403 (2009).

[49] N. Harrison, P. J. W. Moll, S. E. Sebastian, L. Balicas, M. M. Altarawneh, J.-X. Zhu, P. H. Tobash, F. Ronning, E. D. Bauer, and B. Batlogg, Phys. Rev. B **88**, 241108(R) (2013).

[50] D. Aoki, F. Bourdarot, E. Hassinger, G. Knebel, A. Miyake, S. Raymond, V. Taufour, and J. Flouquet, J. Phys.: Condens. Matter **22**, 164205 (2010).

[51] T. D. Matsuda, E. Hassinger, D. Aoki, V. Taufour, G. Knebel, N. Tateiwa, E. Yamamoto, Y. Haga, Y. Ōnuki, Z. Fisk, and J. Flouquet, J. Phys. Soc. Jpn. **80**, 114710 (2011).

[52] J. Béard, J. Billette, M. Suleiman, P. Frings, W. Knafo, G. W. Scheerer, F. Duc, D. Vignolles, M. Nardone, A. Zitouni, P. Delescluse, J.-M. Lagarrigue, F. Giquel, B. Griffe, N. Bruyant, J.-P. Nicolin, G. L. J. A. Rikken, R. B. Lyubovskii, G. V. Shilov, E. I. Zhilyaeva, R. N. Lyubovskaya, and A. Audouard, Eur. Phys. J. Appl. Phys. **59**, 30201 (2012).

[53] S. B. Damelin and W. Miller, *The Mathematics of Signal Processing* (Cambridge University Press, Oxford, UK, 2012).

[54] A. B. Pippard, *Magnetoresistance in Metals* (Cambridge University Press, Cambridge, UK, 1989).

[55] J. M. Ziman, *Electrons and Phonons* (Clarendon Press, Oxford, UK, 1960).

[56] G. W. Scheerer, PhD. thesis, University of Toulouse, 2013.

[57] J. P. Brison, N. Keller, A. Vernire, P. Lejay, L. Schmidt, A. Buzdin, J. Flouquet, S. R. Julian, and G. G. Lonzarich, Physica C **250**, 128 (1995).

[58] In the analysis performed here (Fig. 6), the width of the windows from [13.6 T ; 18.5 T] to [24.1 T ; 32.5 T] was adjusted to correspond to seven periods of the main oscillation ($F_\alpha \simeq$ 1000 T), which is necessary to obtain well-resolved Fourier transforms. At high-field, the Fermi surface is found to be modified in a narrow field window [31.5 T ; 34.7 T], which corresponds to only four periods of the main observed oscillation ($F_\delta \simeq$ 1300 T).